Chemical Engineering Journal 523 (2025) 168932

Contents lists available at ScienceDirect

Chemical Engineering Journal

journal homepage: www.elsevier.com/locate/cej

Nanocomposite kappa-carrageenan-GO/PEI membrane for wastewater valorization and metals recovery

Rokhsare Kardani [a], Ali Altaee [a,*], Armaghan Moghaddam [b], Hossein Ali Khonakdar [c,d,**], Akshaya K. Samal [e], John Zhou [a], Youngwoo Choo [a]

[a] Centre for Green Technology, School of Civil and Environmental Engineering, University of Technology Sydney, 15 Broadway, Sydney, NSW, 2007, Australia
[b] Faculty of Polymer Science, Department of Polyurethane and Advanced Materials, Iran Polymer and Petrochemical Institute (IPPI), Tehran, 14965-115, Iran
[c] Faculty of Polymer Processing, Iran Polymer and Petrochemical Institute (IPPI), Tehran, 14965-115, Iran
[d] Max Bergmann Center of Biomaterials and Institute of Materials Science, Technische Universität Dresden, 01069, Dresden, Germany
[e] Center for Nano and Material Sciences, Jain University, Jain Global Campus, Ramanagara, Bangalore 562112, India

ARTICLE INFO

Keywords:
Hydrogel
Nanocomposite membrane
Heavy metal removal
Nanofiltration
Wastewater
Water purification

ABSTRACT

To address the growing demand for clean water, this study developed a kappa-carrageenan (κC) hydrogel membrane enhanced with graphene oxide (GO) and polyethyleneimine (PEI) for sustainable water purification. GO improved membrane hydrophilicity, permeability, and ion rejection, while PEI enhanced structural stability and selective separation. Spectroscopic, microscopic, water contact angle, tensile strength, and pore size analyses confirmed the membrane's optimized physicochemical properties. The κC-GO.02 membrane with 0.02 % wt/v GO concentration showed optimized performance, with a 20 % increase in pure water flux, from 6.44 to 7.72 L/m^{2}h, due to enhanced pore structure and membrane hydrophilicity. The membrane also demonstrated an outstanding selectivity, rejecting 93 % of NaCl and 97.13 % of $MgSO_4$. Prevalent separation mechanisms included electrostatic repulsion, size exclusion, and surface interactions, where the negatively charged GO surface and PEI functional groups contributed to ion rejection. In the storm wastewater tests, the membrane achieved nearly complete removal of Cd, Zn, Fe, Mn, Cr, Al, B, and Ni, with Pb and Co at 99.7 % rejection and Cu and Li at 94.11 % and 94.48 %, respectively. The material exhibited strong fouling resistance, as reflected by a flux recovery ratio (FRR) of 90.93 % after three filtration cycles, supporting its suitability for scalable and green water treatment processes. With its outstanding permselectivity, the synthesized hydrogel membrane has strong potential for the treatment and recovery of precious metals, such as Li, Co, and Ni, from wastewater treatment for environmental protection and sustainable development.

1. Introduction

Although water is key to economic, cultural, and social development, its availability is increasingly threatened by factors such as urbanization, industrialization, and population growth. These factors have intensified global water usage, creating alarming pressures on the planet's water resources. Issues such as inadequate infrastructure, environmental pollution, ineffective water management, climate change, rising irrigation demands, and unequal water distribution have exacerbated water scarcity. This situation has prompted numerous studies and projects to assess global water demand and availability [1–3]. In response, the use of water purification and desalination technologies has risen significantly, particularly in water-scarce regions. Since the introduction of filtration systems, there has been rapid adoption of membrane separation technologies across various industries, including petroleum, electronics, food, chemicals, pharmaceuticals, and pulp and paper [4].

Membrane materials are broadly categorized into organic and inorganic types. Synthetic polymers, e.g., cellulose acetate (CA), polyethylene, polypropylene, and polytetrafluoroethylene, are commonly used to produce organic membranes [5,6]. Organic polymer membranes are widely studied, and hydrogels in particular are emerging as strong candidates for water treatment technologies. Hydrogel membranes have advantages such as excellent permeability, fouling resistance, tunable selectivity, and versatile applications for desalination and wastewater

* Corresponding author.
** Correspondence to: H. A. Khonakdar, Faculty of Polymer Processing, Iran Polymer and Petrochemical Institute (IPPI), Tehran, 14965-115, Iran.
E-mail addresses: ali.altaee@uts.edu.au (A. Altaee), hakhonakdar@gmail.com (H.A. Khonakdar).

https://doi.org/10.1016/j.cej.2025.168932
Received 21 July 2025; Received in revised form 22 September 2025; Accepted 24 September 2025
Available online 25 September 2025
1385-8947/© 2025 The Author(s). Published by Elsevier B.V. This is an open access article under the CC BY license (http://creativecommons.org/licenses/by/4.0/).

treatment [7,8]. To target emulsified oil and lead ions (Pb^{2+}), a composite hydrogel membrane was prepared by incorporating nano-hydrotalcite and chitosan into polyvinyl alcohol (PVA) [9]. In a chitosan-based membrane, 348.6 L/m^2h.bar water flux, 99.89 % rejection of oil, and 97.44 % rejection of Pb^{+2} were achieved. For landfill leachate treatment, a gravity-fed membrane was constructed from a combination of cellulose, activated carbon, and aluminum hydroxide (CACG) [10]. The CACG membrane exhibited excellent rejection for divalent ions, e.g., 99.9 %, 98.3 %, 96 %, for As^{3+}, Pb^{2+}, and Zn^{2+}, but poorly rejected Na^{+}, 14.9 % only. The hydrogel membrane also persistently rejected 99 % of copper over four filtration cycles, indicating constant membrane performance and reusability. In a study by Ahmad et al. [11], a hydroentangled cotton non-woven membrane was treated with sodium alginate (NaAlg) to create a hydrogel layer within and on the membrane surface for use in water purification. At a NaAlg concentration of 1.5 %, the membrane achieved a water flux of 475 L/m^2·h and effectively separated oil from water, with rejection rates ranging between 97.5 % and 99.5 %.

The exceptional characteristics of kappa carrageenan (κC) hydrogel, such as mechanical strength and adsorption capacity, have attracted the attention of researchers interested in wastewater purification.

Radoor et al. [12] compared the performance of κC- calcium alginate (CaAlg) with lambda carrageenan (λC)-CaAlg (λC-CaAlg) for the treatment of methylene blue (MB). The water flux and rejection rate for the κC-CaAlg hydrogel, 11.19 L/m^2 h and 99.22 %, were lower than what was observed for the λC-CaAlg hydrogel, 11.67 L/m^2 h and 100 %.

Zhao et al. [13] developed a graphene oxide (GO)-reinforced calcium alginate (GO-CaAlg) membrane to enhance the antimicrobial properties and reduce swelling typically observed in pure calcium-based hydrogel membranes. The membrane achieved a 97 % rejection rate for Coomassie Brilliant Blue (CBB) dye, while the rejection of NaCl remained low at approximately 8 %. Water flux recovery of the GO-CaAlg was 97 %, indicating outstanding membrane antifouling properties. Surface modification of nanofiltration (NF) membrane using κC- GO and crosslinked by glycerol was investigated by Sudesh et al. [14]. The optimized antifouling NF membrane attained 95 % rejection of $MgSO_4$, 23 % of NaCl, and a 58 L/m^2h maximum pure water flux. The membrane showed excellent water flux recovery of 95.73 % after wastewater treatment, demonstrating the ability to overcome membrane fouling. Despite their outstanding water flux and dye rejection, hydrogel membranes exhibited a low rejection of monovalent and divalent ions. This made the membrane less suitable for general wastewater treatment in particular. Besides, the research performed about κC development into hydrogel membranes is still limited despite its unique characteristics of mechanical stability and adsorption to heavy metals.

This study investigated the potential to design and develop a κC hydrogel membrane with a high rejection rate to divalent and monovalent ions for wastewater treatment. κC was selected due to its thermal and mechanical stability, abundance of sulfate and hydroxyl functional groups, biodegradability and environmental compatibility, and tunable mechanical strength via crosslinking, making it a sustainable and versatile candidate for water treatment applications [67]. GO was incorporated into the κC hydrogel to improve the membrane antifouling properties and rejection. The membrane dope was cast on a 0.2 μm CA support layer and crosslinked with polyethyleneimine (PEI) to reduce the membrane swelling that could lead to its detachment from the base support layer. Structural and morphology analyses characterized the fabricated hydrogel membrane. Water uptake, swelling degree, porosity, and pore radius were measured for all κC-GO/PEI membranes. Membrane rejection, water flux, and membrane fouling were also measured. Repeated filtration runs were performed to examine the membrane's long-term stability.

2. Materials and methods

2.1. Materials

All reagents used in this research were analytical grade and employed as received, without any further purification. κC, a sulfated plant polysaccharide, and branched PEI with an average molecular weight of 25,000 g/mol were sourced from Sigma-Aldrich (Australia). GO with a large surface area (Brownish Yellow Powder; Oxygen Content: ~40.78 wt%; BET Surface Area: >100 m^2/g; Lateral Size: 1–5 μm; Thickness: 0.8–1.2 nm) was obtained from ACS Material, LLC, USA.

The stormwater samples in this study were collected from Leumeah, 2560, New South Wales, filtered through a 0.45 μm CA membrane (Thermo Fisher Scientific, Sartorius Stedim Biotech GmbH, Germany) for the removal of relatively large particles, such as organic and inert matters, and stored in a refrigerator at 4 oC. The stormwater was used without any modifications to the solution concentration or pH to resemble field conditions, where the natural pH governs metal speciation and rejection. Table 1 outlines an overview of the characteristics of the storm wastewater used in this research. To assess the rejection of ions by the fabricated membranes, model solutions were prepared by dissolving magnesium sulfate ($MgSO_4$) and sodium chloride (NaCl) in deionized (DI) water. These salts were obtained from Sigma-Aldrich (Australia). A CA filter paper with a 0.2 μm pore size (Thermo Fisher Scientific, Sartorius Stedim Biotech GmbH, Germany) served as the membrane's support layer. The CA membrane would have no impact on the molecular weight cut-off of the κC-GO/PEI membrane that was developed for rejecting ions.

2.2. Preparation and performance studies

A 3 % (wt/v) solution of κC was prepared by dissolving the polymer powder in DI water at 60 °C, and stirring continuously for 3 h until a homogeneous gel-like solution was obtained. Previous studies showed that 3 % κC has the best performance when used in filtration processes [15]. After cooling, the solution was blended at 450 rpm for 1 h to increase its surface area by mechanical fragmentation and facilitate the hydrogel's even distribution in the solution or composites. Separately, GO solutions were prepared at concentrations of 0.01 %, 0.02 %, 0.03 %, and 0.04 % (wt/v) by dispersing the GO powder in DI water. Each solution was mixed at room temperature under constant stirring for 1 h,

Table 1
Storm wastewater characteristics.

Parameter	Value
Appearance	Light yellow color
Conductivity	454.7 ± 15 μS/cm
Total Organic Carbon (TOC)	37.63 ± 3 mg/L
Total Dissolved Solids	430.7 ± 10 mg/L
pH	5.31
Turbidity	11.9 ± 3 NTU
Salinity	422.8 ± 10 mg/L
Total Suspended Solids	10.6 ± 2 mg/L
Mg	18.63 ± 2 mg/L
Ca	11.15 ± 2 mg/L
Na	69.76 ± 5 mg/L
Cl	68.83 ± 5 mg/L
Cd	0.8 ± 0.1 mg/L
Pb	0.78 ± 0.1 mg/L
Al	0.45 ± 0.1 mg/L
Cr	0.525 ± 0.1 mg/L
Mn	0.8 ± 0.1 mg/L
Li	0.84 ± 0.1 mg/L
Co	0.77 ± 0.1 mg/L
Ni	0.76 ± 0.1 mg/L
Cu	0.82 ± 0.1 mg/L
Zn	0.8 ± 0.1 mg/L
Fe	0.23 ± 0.1 mg/L
B	0.48 ± 0.1 mg/L

followed by 3 h of sonication in an ultrasonic bath (Powersonic, Digital Ultrasonic Bath) operating at 40 kHz, with the temperature maintained between 40 and 45 °C to ensure complete dispersion. A 2 % (wt/*v*) PEI solution was also prepared separately by dispersing PEI in DI water under continuous stirring for 15 min until a homogeneous mixture was obtained. Negatively charged κC and positively charged PEI form a strong ionic crosslinking besides the hydrogen bonding that further stabilizes the hydrogel network [16].

For preparing the dope solution (Fig. 1), 3 mL of the 3 % κC solution was first poured into a small bottle and maintained at 60 °C. Once fully homogenized, 0.1 mL of the 2 % PEI solution was added to the bottle and allowed to crosslink for 1 h. Following this, 10 mL of the GO solution was gradually introduced, with continuous stirring at 750 rpm and sonication to ensure uniform dispersion. A 0.2 μm pore-sized CA filter paper was provided as the support layer. To enhance adhesion, 1 mL of 2 % PEI solution was applied to the filter paper and left to dry. PEI and CA contain hydroxyl (-OH) and carbonyl (C=O) groups that facilitate strong hydrogen bonding between the polymer composite (PEI–κC) and the CA support. In addition, CA carries residual negative charges that would electrostatically interact with the PEI positive charge. The CA filter paper was then placed at the bottom of a Sterlitech HP4750 dead-end filtration cell (Sterlitech, USA), and the prepared dope solution was introduced under a hydraulic pressure of 5 bar for 2 h. Finally, the fabricated membrane was removed and dried at 50 °C for 2 h to ensure proper structural stability. Table 2 presents the formulations of all fabricated membranes.

Pure water flux experiments were conducted at ambient temperature. The experimental setup included an HP4750 dead-end filtration unit (Sterlitech) with a 300 mL feed chamber and a membrane surface area of 14.6 cm^2. Prior to data collection, membranes were stabilized through a 30-min compaction phase. The water flux (J) was calculated using Eq. (1), where *V* represents the volume of collected permeate (L), A denotes the membrane's effective area (m^2), and t is the filtration duration (h):

$$J = \frac{V}{A^*t} \tag{1}$$

Contaminant rejection, including NaCl, $MgSO_4$, and storm wastewater, was assessed by measuring the concentration of solutes in the permeate and feed solutions. Rejection efficiency (% R) was determined using the formula provided in Eq. (2):

$$R = \left(1 - \frac{C_p}{C_f}\right)^*100 \tag{2}$$

Here, Cf and Cp represent the solute concentrations in the feed and permeate solutions (mg/L). Heavy metal levels were measured by inductively coupled plasma mass spectrometry (ICP-MS). All experiments were conducted at 3 bar pressure and repeated for three cycles to ensure reliability. For the heavy metal rejection studies, stormwater was collected and used as the feed without further dilution, with its characteristics detailed in Table 1.

The antifouling behavior of the composite membranes was assessed using the previously mentioned filtration setup. The tests were conducted with storm wastewater as the feed solution. All tests were conducted under a steady pressure of 3 bar, with an active surface area of 14.6 cm^2. First, DI water flux (J_1) was measured. Then, storm wastewater was served as the feed to record the permeate water flux (J_P) in a dead-end filtration setup. Afterward, the membranes were rinsed with DI water, and the post-cleaning water flux (J_2) was measured again with DI water. The same procedure was applied to storm wastewater samples. The reversible (R_r), irreversible (R_{ir}), total fouling (R_t), and fouling recovery ratio (FRR) were determined using Eqs. (3)–(6):

$$R_r\ (\%) = \left(\frac{J_2 - J_p}{J_1}\right) \times 100 \tag{3}$$

$$R_{ir}\ (\%) = \left(\frac{J_1 - J_2}{J_1}\right) \times 100 \tag{4}$$

Table 2
Formulation of fabricated membranes.

No.	Membrane	κC (% wt/v)	GO (% wt/v)	PEI 2 % wt/v (aq sol, ml)
1	κC	3	0	0.1
2	κC-GO.01	3	0.01	0.1
3	κC-GO.02	3	0.02	0.1
4	κC-GO.03	3	0.03	0.1
5	κC-GO.04	3	0.04	0.1

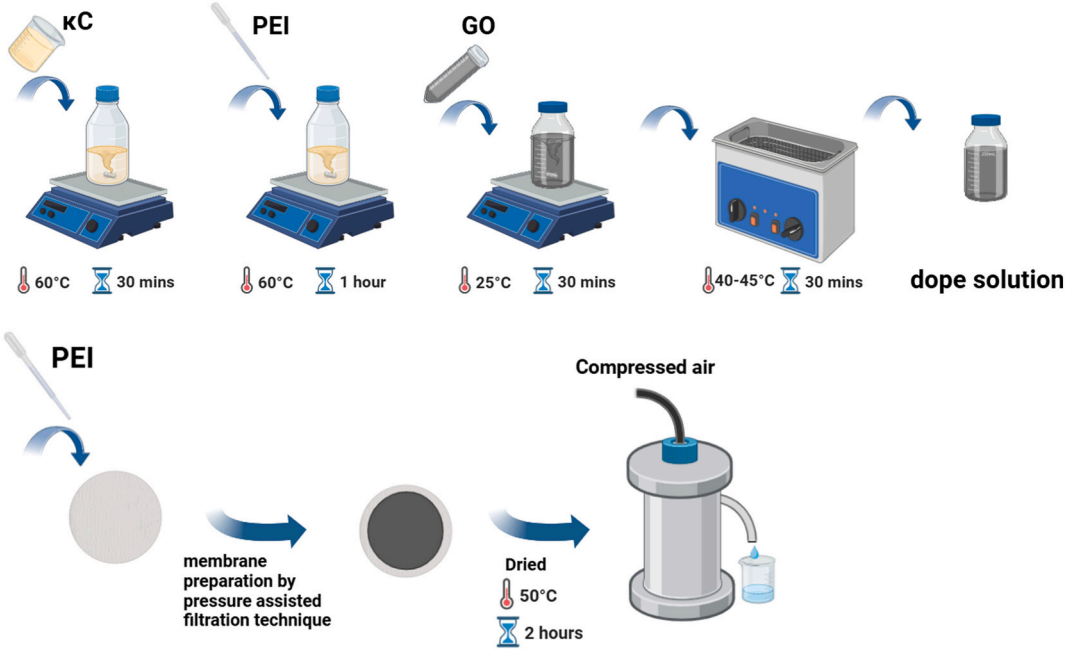


Fig. 1. Membrane Fabrication and Testing.

$$R_t\ (\%) = \left(1 - \frac{J_P}{J_1}\right) \times 100 \quad (5)$$

$$FRR\ (\%) = \left(\frac{J_2}{J_1}\right) \times 100 \quad (6)$$

2.3. Analytical methods

The surface morphology of the membranes was analyzed using Field Emission Scanning Electron Microscopy (FESEM) with a Zeiss EVO LS15 SEM (Zeiss, Sydney, Australia). In addition, Energy Dispersive X-ray (EDX) (Bruker SDD XFlash 5030 detector, Zeiss, Australia) was performed to analyze the heavy metals captured by the samples. The membranes were pre-treated by drying and then coated with a conductive film to eliminate charging effects. Cross-sectional imaging was also conducted to investigate the membrane structure further. X-ray diffraction (XRD) analysis was performed using a Bruker D8 Discover diffractometer (Bruker, Australia) equipped with Cu Kα radiation (λ = 1.5406 Å). The dried membranes were analyzed within a 2θ angular range of 10° to 80°, and the interlayer distance (d-spacing) was determined based on Bragg's equation.

Fourier Transform Infrared Spectroscopy (FTIR) was conducted to identify the functional groups in the membrane samples. A Thermo Scientific Nicolet spectrometer, featuring an optical resolution of 0.9 cm^{-1}, coupled with an infrared microscope (Thermofisher, Sydney, Australia), was employed. The samples underwent drying at 50 °C for two hours before FTIR analysis, which spanned a wavenumber range of 4000 to 500 cm^{-1}. Three scans were averaged to produce the final spectra.

To evaluate the water absorption capacity of the membranes, their mass was measured before and after soaking in distilled water for 24 h at ambient temperature. First, the dry weight (W_A) of each membrane was obtained by drying it in an oven at 50 °C for 3 h. After immersion, the wet weight (W_B) was recorded, and water uptake (WU) was calculated using Eq. (7).

$$WU = \frac{(W_B - W_A)}{W_A} * 100 \quad (7)$$

Swelling behavior was assessed by determining the swelling degree (SD) of the membrane. The initial thickness of the membrane (T_i) was recorded, and the membrane was soaked in distilled water for 2 h. After measuring the final thickness (T_f), the swelling degree was calculated as:

$$SD = \frac{(T_f - T_i)}{T_i} \quad (8)$$

The wettability of the membranes was evaluated through the sessile drop technique by placing a water droplet on the membrane surface and recording the contact angle. Three different spots on each membrane were tested, and the average contact angle (WCA) was recorded. Ion concentration in the feed and permeate was quantified by Inductively Coupled Plasma Mass Spectrometry (ICP-MS) (Agilent Technologies), with samples being analyzed for heavy metal rejection efficiency.

Zeta potential of dope solution dispersions was determined by electrophoretic light scattering using a Nano-ZS Zetasizer (Malvern Analytical, UK) with disposable capillary cells. Measurements were conducted in deionized water at room temperature, and values are reported as the average of six runs per sample.

To assess the porosity of the hydrogel membranes, a gravimetric analysis was performed. Samples were first saturated by soaking in DI water for 24 h, after which their hydrated mass (W_{wet}) was measured. Subsequently, the membranes were dehydrated in a controlled-temperature oven at 50 °C for 4 h to obtain their anhydrous mass (W_{dry}). The porosity percentage (p%) was then determined through the following equation:

$$p\% = \frac{W_{wet} - W_{dry}}{A \times l \times \rho} \quad (9)$$

Here, A refers to the surface area of the membrane (cm^2), l indicates the membrane's thickness (cm), and ρ stands for the density of water, taken as 1 g/cm^3.

The mean pore size of the membranes was determined through analysis of their porosity and water flux, employing the following equation:

$$r = \sqrt{\frac{(2.9 - 1.75p) \times (8 \times lQ\eta)}{P \times A \times \Delta P}} \quad (10)$$

The volumetric flow rate of pure water (Q, in m^3/s), along with the water viscosity (η = 0.00089 Pa·s), membrane porosity (p), effective surface area (A), membrane thickness (l), and applied pressure difference (ΔP), were used to calculate the average pore radius.

Tensile strength testing was assessed with a Universal Testing Machine (LLOYD, AMETEK, UK) equipped with a 1 kN load cell. Membranes were cut into rectangular strips with a width of 1 cm and mounted vertically between the grips with a gauge length of 30 mm. The test was conducted at room temperature with a constant crosshead speed of 10 mm/min. Each sample was tested in triplicate, and the average tensile strength was calculated. Stress values were obtained by dividing the maximum load by the cross-sectional area of the membrane.

Finally, the average molecular weight between crosslinks (M_C) of the hydrogel membranes was calculated using the Flory–Rehner equation, based on WU measurements (see Supplementary Material for details).

3. Results and discussions

3.1. Physicochemical properties

3.1.1. FTIR and XRD

The FTIR spectra offer an understanding of the chemical interactions of the membrane components. In Fig. 2a, the FTIR spectrum of the κC membrane showed explicit peaks around 1400 cm^{-1} (C—H bending), 1500 cm^{-1} (N—H bending), and 600 cm^{-1} (N—H out-of-plane bending), characteristic of PEI, reflecting the presence of its amine groups [17]. κC contributed to the presence of a broad peak around 3600 cm^{-1} (O—H stretching) and distinct peaks at 840 cm^{-1} (C-O-SO_3^-), 900 cm^{-1} (C-O-C), and 1200 cm^{-1} (S=O), indicative of its sulfated polysaccharide structure [15]. CA was identified by its strong peaks at 1740 cm^{-1} (C═O stretching), 1230 cm^{-1} (C-O-C stretching), and 1037 cm^{-1} (C—O stretching), corresponding to its acetate groups [18]. Additionally, the peak at 1370 cm^{-1} arose from C—H bending vibrations in the alkyl chains shared by all components. These peaks collectively elucidated the chemical structure and interactions within the membrane.

At low GO loadings (κC-GO.01 and κC-GO.02), the increased intensity of the O—H stretching vibrations in the 3500–3800 cm^{-1} region indicated enhanced hydrogen bonding between GO's hydroxyl groups and the polymer composite matrix (kC and PEI), leading to improved hydrophilicity. This enhancement is critical for water permeability and ion rejection [19]. In the 1300–1600 cm^{-1} region, the peaks corresponding to N—H bending (1500 cm^{-1}) and C—H bending (1400 cm^{-1}) became sharper (Fig. 2b), showing enhanced electrostatic interactions between κC and PEI, as well as hydrogen bonding with GO, indicating stronger network formation [20].

However, at higher GO loadings (κC-GO.03 and κC-GO.04), the spectra in these regions began to resemble that of the pure membrane (kC without GO), likely due to GO aggregation or saturation of interaction sites. This aggregation reduced the availability of functional groups for hydrogen bonding and electrostatic interactions, potentially diminishing the membrane's performance due to partial loss of effective crosslinking.

FTIR spectra before and after filtration showed only very minor

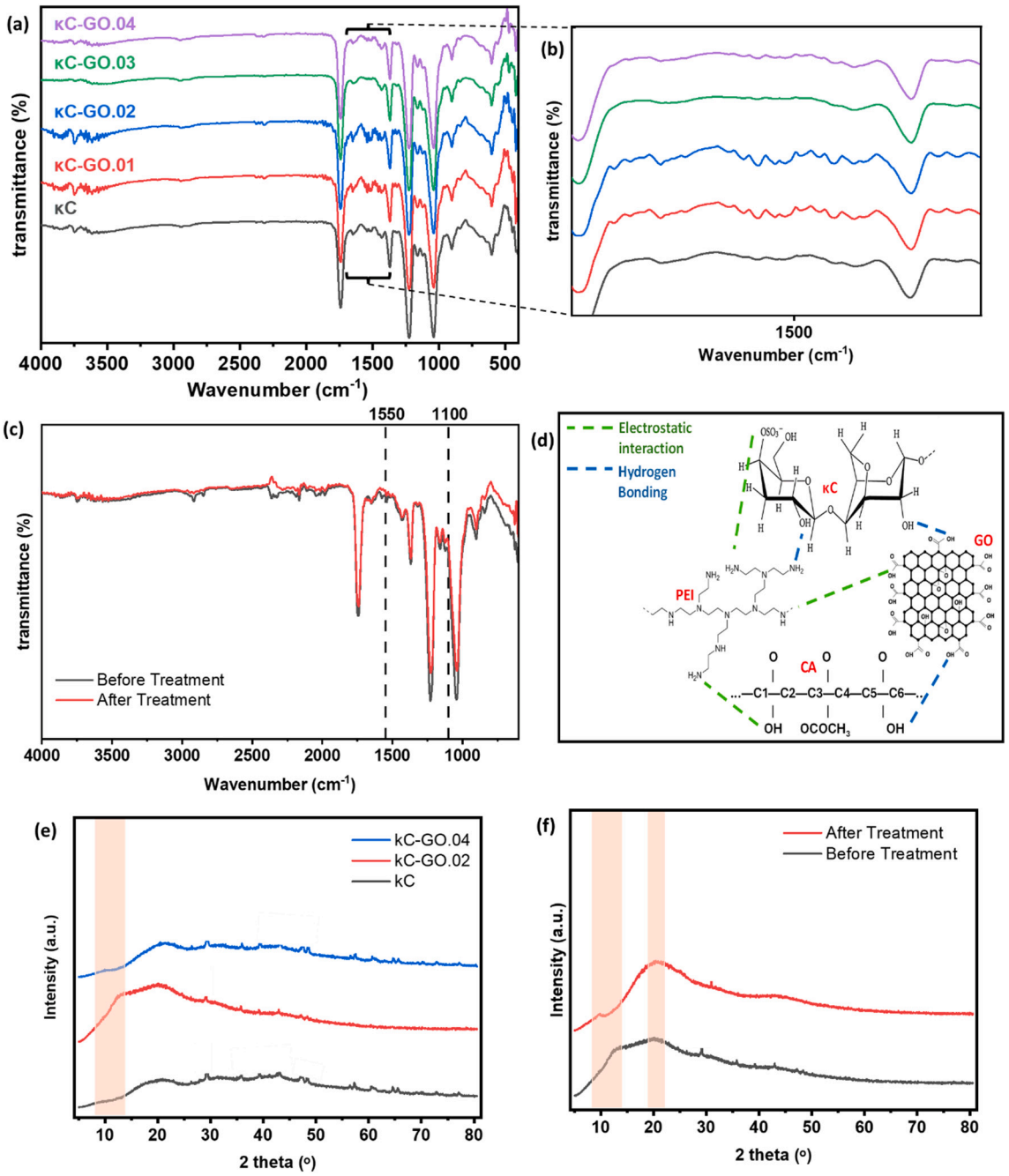


Fig. 2. (a) FTIR spectra of the κC and κC loaded with GO, (b) Zoomed-in FTIR spectra (1300–1600 cm^{-1}), (c) FTIR spectra of the κC-GO.02 before and after treatment with storm wastewater, (d) Molecular interactions within the components. (e) XRD analysis of κC, κC-GO.02, κC-GO.04 (f) XRD analysis of κC-GO.02 before and after treatment with storm wastewater.

changes, indicating that the κC-GO.02 membrane resisted significant foulant accumulation. After filtration, a small increase was detectable around 1550 cm^{-1} (amide II/organic species) and a very slight change in the ~1100 cm^{-1} region (C–O/Si–O/PO_4^{3-} contributions), consistent with trace organic and colloidal deposition. Importantly, no strong new carbonyl (~1700 cm^{-1}) or carbonate (~1420, 870 cm^{-1}) bands were observed, confirming that irreversible fouling was minimal. These subtle spectral variations were consistent with the high flux recovery and low R values, demonstrating that fouling was limited and largely reversible.

XRD results in Fig. 2e highlighted the structural changes induced by increasing GO content in the membrane composition. κC-GO.02 exhibited a broad peak at 12.43°, indicating good dispersion and intercalation of GO within the κC matrix. Compared to the membrane with no GO, which showed broader and less intense features. At higher GO loading (κC-GO.04), the peak shifted slightly toward 10° and resembled the κC membrane, suggesting GO agglomeration and partial stacking.

The XRD analysis of the membrane, both before and after wastewater treatment, illustrated in Fig. 2f, reveals slight structural modifications in GO and κC. Before the treatment, GO exhibited a characteristic peak at 12.43° with a d-spacing of 7.12 Å, which shifted to 9.82° after treatment, corresponding to an increased d-spacing of 9.00 Å. This shift suggested an expansion of the GO interlayer spacing, likely caused by the entrance of water and the adsorption of ionic or organic species present in storm wastewater. These species had the potential to penetrate GO galleries, leading to structural expansion detectable by XRD [21]. For κC, the

characteristic peak at 20.16° (d-spacing 4.40 Å) remained nearly unchanged after treatment, shifting slightly to 20.41° (d-spacing 4.35 Å). This minimal change suggested that the polysaccharide backbone of the κC matrix retained its semi-crystalline structure and resisted degradation during filtration, indicating its good physical and chemical stability of the κC matrix under application conditions and its responsiveness to environmental exposure.

3.2. Hydrophilicity and surface properties

3.2.1. Water uptake and swelling degree

The water uptake of the membranes was determined by measuring their weight before and after immersion in distilled water for 24 h at room temperature. The swelling degree of the membranes was evaluated by measuring their thickness before and after immersion in distilled water for 2 h. As shown in Fig. 3a, the water uptake capacity and swelling degree of the composite hydrogels increased with the addition of GO. The pure κC membrane exhibited a water uptake of 842.85 % and a swelling degree of 3.7, consistent with the inherent hydrophilicity of κC due to its hydroxyl (-OH) and sulfate (-SO_3^-) groups, which form strong hydrogen bonds with water molecules. With the addition of GO in κC-GO.01, the water uptake increased to 1166.67 %, and the swelling degree rose to 4.05, indicating that the well-dispersed GO sheets introduced additional hydrophilic sites. Functional groups such as hydroxyl (-OH) and carboxyl (-COOH) groups, combined with the inherent hydrophilic nature of κC, provided additional sites for hydrogen bonding with water, leading to enhanced water absorption and swelling. The observed increased water uptake and swelling degree exhibited the role of GO in enhancing the membrane's hydrophilicity and structural modifications further. This trend continued in the κC-GO.02 sample, where the water uptake reached 1200 %, and the swelling degree increased to 4.63. At higher GO loadings, both water uptake and swelling degree continued to rise, but at a slower rate. For κC-GO.03, the water uptake was 1218 %, and the swelling degree was 4.78, while for κC-GO.04, these values reached 1228.57 % and 4.94, respectively. This plateau in both water uptake and swelling degree could be attributed to GO aggregation (which limited their effective dispersion and interaction), increased crosslinking density, reduced pore size, and saturation of hydrophilic sites. The overall increase in water uptake and swelling degree highlighted the role of GO in enhancing the membrane's hydrophilicity.

Moreover, the increased surface area of GO nanosheets could create more opportunities for water–material interactions at the nanoscale. In addition to hydrophilicity, the incorporation of GO also appeared to influence the physical structure of the membrane matrix. At lower loadings, GO could act as a spacer that interfered with dense chain packing and formation of a network with a high density of crosslinks, leading to a more flexible network with wider pores that allowed more water molecules to penetrate and expand the structure. The interaction between κC and GO, which likely occurred via hydrogen bonding and electrostatic interactions, helped with maintaining the structural cohesion at low GO loading, while permitting high swelling and water uptake [22–25].

3.2.2. Water contact angle

The water contact angle of the membranes decreased significantly with the incorporation of GO (Fig. 3b), reflecting the enhanced hydrophilicity of the membranes. The pure κC membrane exhibited a WCA of 68.51°, indicating moderate hydrophilicity due to the presence of hydroxyl (-OH) and sulfate (-SO_3^-) groups in κC. With the addition of GO in κC-GO.01, the WCA decreased to 58.75°, demonstrating that the well-dispersed GO sheets introduced additional hydrophilic functional

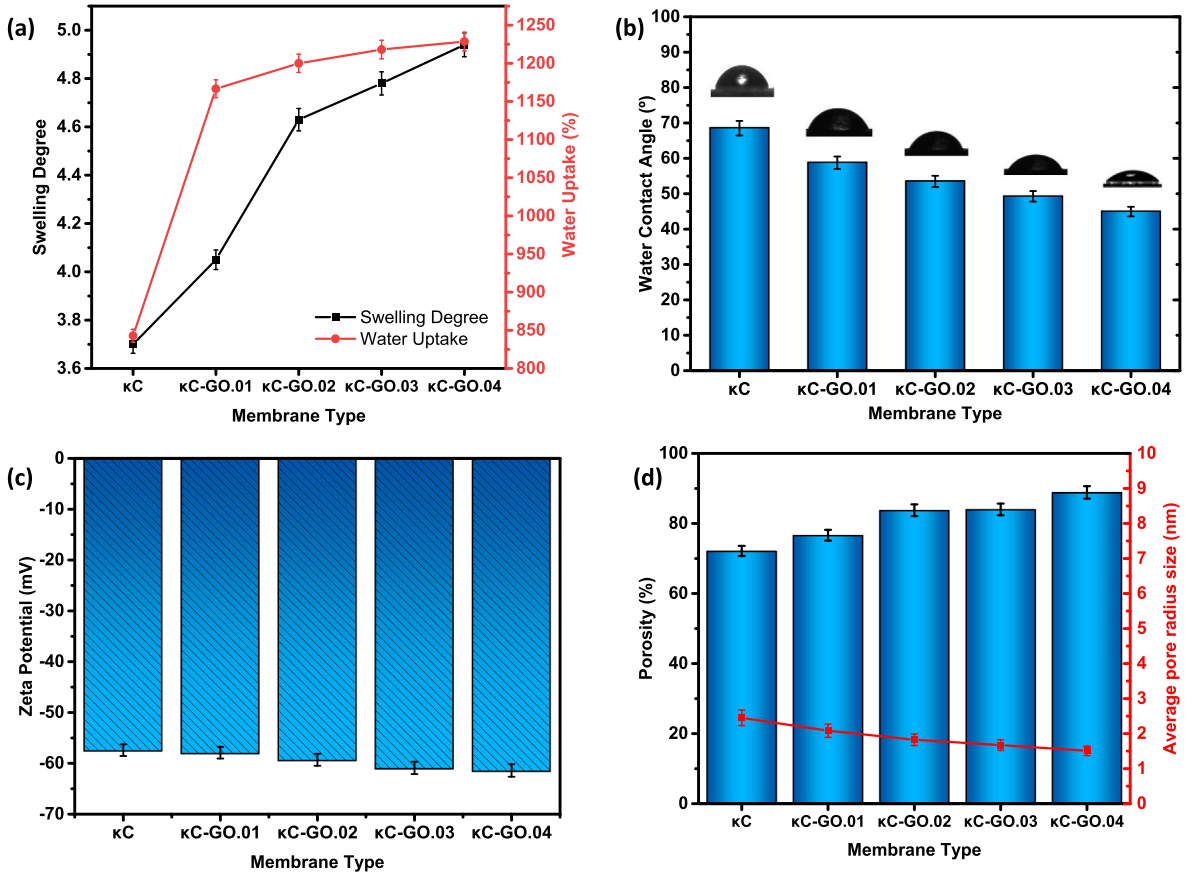


Fig. 3. (a) Swelling degree and water uptake, (b) Water contact angle, (c) Zeta potential, (d) Porosity and average pore radius size of different membranes.

groups, such as hydroxyl (-OH) and carboxyl (-COOH), which improved the membrane's affinity for water [26]. This trend continued in κC-GO.02, where the WCA further decreased to 53.47°, suggesting an optimal dispersion of GO within the polymer matrix and maximal enhancement of hydrophilicity. At higher GO loadings, the WCA continued to decrease but at a slower rate. For κC-GO.03, the WCA was 49.26°, while for κC-GO.04, it reached 44.95°. At higher GO concentrations, the enhancement in hydrophilicity became less pronounced, which could be related to the partial aggregation or stacking in GO nanosheets. These aggregates could reduce the effective interactions of functional groups on the sample surface. Nevertheless, the overall observed trend confirmed that increasing the GO content improved surface hydrophilicity. This increase in hydrophilicity was also consistent with the observed enhancement in swelling degree at higher GO loadings.

3.2.3. Zeta potential

As shown in Fig. 3c, the pure κC membrane exhibited a zeta potential of −57.4 mV, reflecting the negative sulfate (-SO_3^-) groups of κC. With the incorporation of GO, the zeta potential values became slightly more negative across the membranes: κC-GO.01 (−57.9 mV), κC-GO.02 (−59.3 mV), κC-GO.03 (−60.9 mV), and κC-GO.04 (−61.4 mV). While the net zeta potential values increased and became more negative, the overall changes were relatively small, indicating that GO enhanced the negative surface charge of the membranes to a limited extent. This increase in negative charge could be attributed to the introduction of additional negatively charged functional groups, such as carboxyl (-COOH) and hydroxyl (-OH), from GO [27,28]. However, the presence of polyethyleneimine (PEI) in all membranes played a significant role in limiting the extent of this increase. The positively charged amine groups (−NH2) of PEI partially neutralized the negative charges of both κC and GO, resulting in a small net increase in zeta potential (more negative) [29]. Accordingly, the results further confirmed that GO was incorporated into the polymer network and contributed to the overall electrostatic environment, which could indirectly influence the polymer interactions and network organization. All membranes maintained a strongly negative zeta potential (below −50 mV), beneficial for repelling negative ions and foulants and improving antifouling properties [30].

3.3. Morphological analysis

3.3.1. Porosity and pore size

Fig. 3d illustrates the GO loading effect on the porosity and pore size of membranes. The porosity of the membranes increased from 72.14 % for pristine κC to 76.64 %, 83.76 %, 84.00 %, and 88.86 % for κC-GO.01, κC-GO.02, κC-GO.03, and κC-GO.04, respectively. The increase in porosity with GO incorporation could be attributed to several factors. Firstly, the high monolayer content of GO (~99 %) and high oxygen functionality (~40.78 wt%) introduce abundant hydrophilic functional groups (-OH, -COOH, -C=O), which enhance the interaction between GO and the polymer matrix, leading to structural modifications that generate additional voids [31,32]. Secondly, the lateral size of GO (1–5 μm) facilitates the formation of an expanded network within the polymer matrix, preventing excessive compaction and maintaining high porosity. Additionally, the high density of GO (~270 g/L) allows for effective dispersion at lower concentrations, promoting a more porous morphology [33].

Despite the increase in porosity, the calculated average pore size of the membranes decreased from 2.45 nm for pristine κC to 2.08 nm, 1.82 nm, 1.67 nm, and 1.51 nm for κC-GO.01, κC-GO.02, κC-GO.03, and κC-GO.04, respectively. The results revealed that the hydrogel membranes' porosity increased with GO concentration, while pore size decreased as the GO concentration increased. The reason for the porosity increase was attributed to the formation of interconnected nanochannels and interlayer gaps between the GO sheets. Contrarywise, pore size decreased due to the GO deposition on the pore wall, narrowing existing pores and subdividing them into smaller channels [34,35].

The observed trends could suggest that GO planes interfered with the dense packing of polymer chains, leading to the formation of a more open matrix. The planar structure of GO could act as a physical spacer, disrupting chain entanglements and increasing the overall void volume. Thus, the total porosity increased, despite observing a reduction in average pore size. This behavior could be attributed to the formation of a higher number of pores, which were smaller in size, as the GO nanosheets prohibited pore growth while preventing the compaction of the polymer matrix [36–38]. It was expected that the enhanced porosity could improve water permeability by increasing the number of water transport pathways and reducing overall hydraulic resistance, as later observed in membrane performance tests.

3.3.2. SEM and EDX

The SEM images of membranes, shown in Fig. 4, highlight significant changes in morphology due to the incorporation of GO. The pure κC membrane exhibits a smooth, compact surface typical of a dense polymer matrix, which limits water flux. However, upon the addition of GO, the surface becomes visibly rougher and more porous, indicating the successful integration of GO into the κC matrix. This increase in surface roughness is associated with enhanced membrane hydrophilicity, leading to improved water flux and antifouling characteristics, as the rougher surface provides more pathways for water flow and reduces fouling potential. GO disrupted polymer packing during drying, leading to a more porous structure with better mechanical stability and expected improvement in water permeability [39,40]. At moderate GO loadings, the morphology appeared uniform, suggesting good interfacial compatibility between κC and GO. However, at higher GO content, for example, κC-GO.04, agglomeration occurs, leading to localized irregularities. Such clusters could create non-uniform transport pathways and compromise membrane homogeneity, mechanical stability, and efficiency.

The cross-sectional SEM image of κC-GO.02 revealed a bilayer membrane structure, with clear contrast between the porous CA support and the denser hydrogel-based selective layer. This layered architecture reflected a successful casting process for forming a uniform and continuous selective layer. The uppermost region of the CA paper exhibited a gradation in contrast, becoming more similar in shade to the overlying hydrogel, which could indicate partial interpenetration and diffusion of the hydrogel layer into the top layer of the CA support. This morphological evidence suggested an intimate interfacial contact rather than a sharply delaminated boundary. The membrane thickness was measured using ImageJ software, confirming an average thickness of approximately 34 μm.

EDX analysis confirmed the successful capture of various heavy metals and ions on the membrane surface after storm wastewater treatment. Elements such as aluminum, magnesium, nickel, chloride, manganese, sodium, iron, lead, and copper were detected following the membrane treatment. These findings demonstrated the membrane's ability to adsorb and retain heavy metals effectively. The observed increase in oxygen content suggested the formation of surface-bound metal oxides or hydroxide complexes. The reported values in Table 3 represent the average composition from multiple measurements.

These findings also indicated that fouling was dominated by inorganic/metallic deposition and cation exchange processes, consistent with the stormwater composition and the high rejection of divalent and multivalent cations observed in the performance tests.

3.4. Mechanical properties

The incorporation of GO into κC-based membranes significantly improved their tensile strength. As shown in Fig. 5, the pristine κC membrane exhibited a tensile strength of 13.67 MPa. With the addition of 0.01 wt% GO, the tensile strength increased to 16.33 MPa. A further improvement in the tensile strength was recorded when the GO

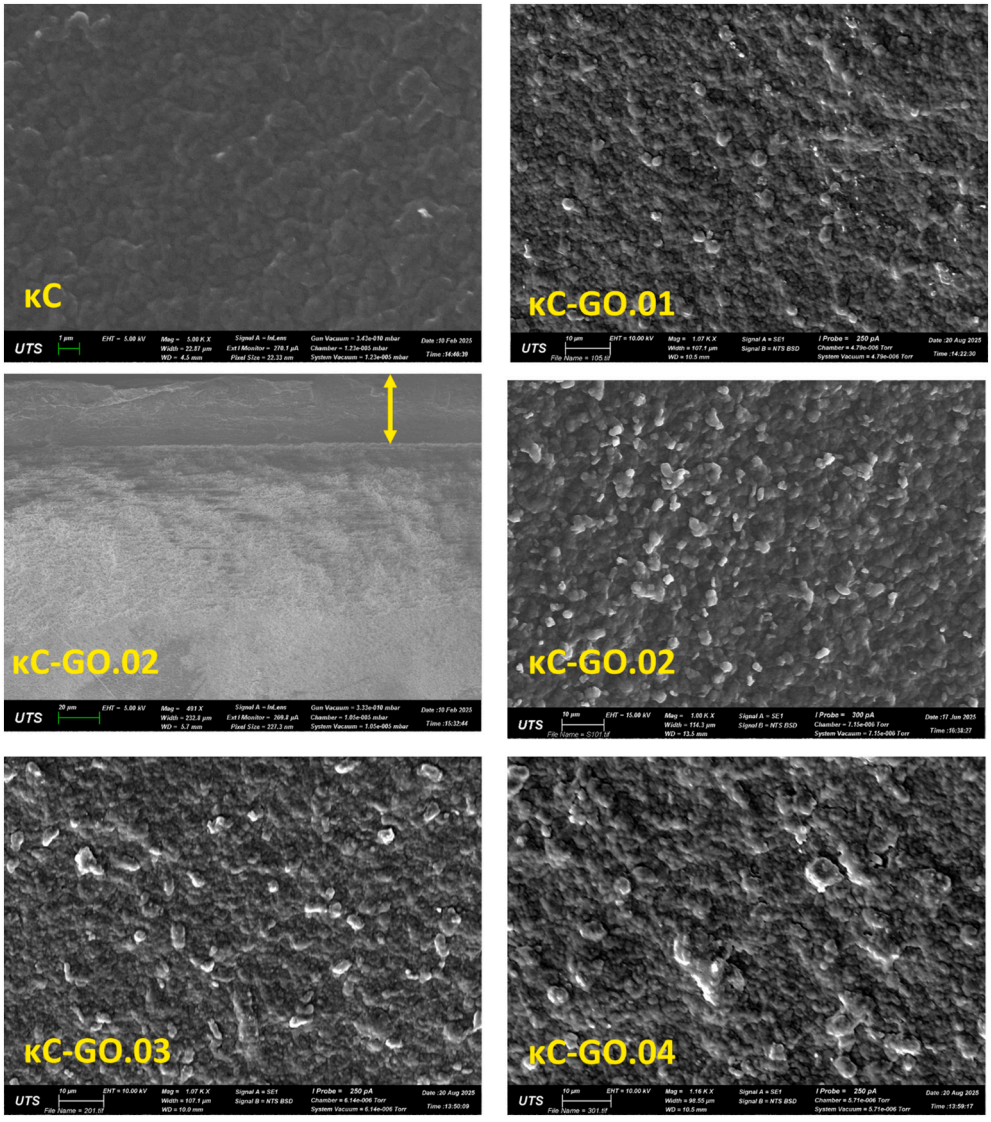


Fig. 4. SEM analysis of different membranes.

Table 3
Elemental analysis using EDX to assess changes in κC-GO.02 membrane composition before and after treatment.

Sample	Elemental Composition (wt%)											
	C	O	S	K	Al	Mg	Na	Cl	Fe	Mn	Pb	Cu
κC-GO.02 before treatment	13.33	28.56	17.16	6.87	–	–	–	–	–	–	–	–
κC-GO.02 after treatment	14.19	35.95	19.52	1.26	0.17	0.73	0.15	1.02	0.46	0.14	0.66	0.48

concentration increased to 0.02 wt% in the κC-GO.02 membrane, which achieved a tensile strength of 19.65 MPa, showing a 43 % improvement in the tensile strength compared to the pure κC membrane. However, increasing the GO content beyond 0.02 wt% resulted in a slight decrease in tensile strength, with the κC-GO.03 and κC-GO.04 membranes showing 18.45 MPa and 17.53 MPa, respectively. This trend suggested that while GO enhanced the mechanical properties of the membranes, since GO nanosheets are prone to clustering at higher concentrations, aggregation occurred at high GO contents, leading to a reduction in the uniform distribution and load-bearing capacity of the GO sheets [41]. Thus, the optimal GO concentration for maximum tensile strength appears to be 0.02 wt%.

The observed changes in mechanical properties could also be linked to the changes in porosity. While a moderate enhancement in porosity could support better stress distribution by permitting some energy dissipation, excessive porosity caused the formation of structural weak points. In other words, GO contents increased the porosity at the expense of cohesive strength. Therefore, it could be said that for the κC-GO.02 sample, a balance was achieved: the low GO concentration provided both improved mechanical reinforcement and moderate porosity, showing the best compromise between enhanced porosity and uniform structural reinforcement. In addition, the observed trend in mechanical properties was also related to M_C values for each hydrogel sample, as discussed in the Supplementary Material.

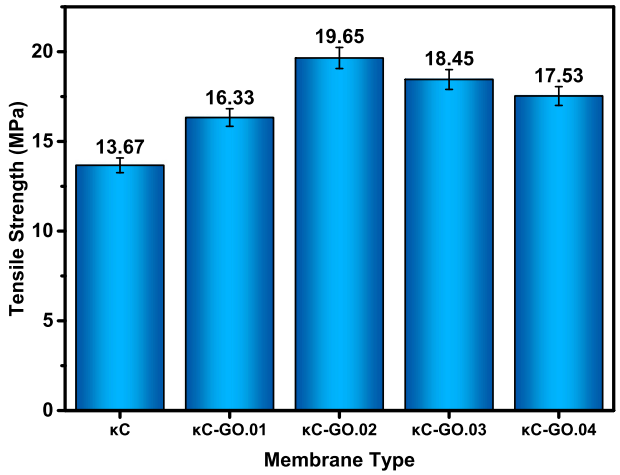


Fig. 5. Tensile strength of κC-GO membranes with varying concentrations of GO.

3.5. Performance studies

3.5.1. Water flux and rejection

The pure water flux of κC and κC-GO membranes was evaluated to assess the impact of GO on membrane performance. All tests were conducted at 3 bar hydraulic pressure and a room temperature of 22 °C. Water flux results showed a gradual increase of 31 %, from 6.44 ± 0.15 L/m^{2}h for the κC to 8.45 ± 0.17 L/m^{2}h for the kC-GO.04, confirming the positive effect of GO incorporation on water permeability (Fig. 6a). The enhancement in water flux could be attributed to the polar oxygen-containing functional groups in GO, such as hydroxyl (-OH), carboxyl (-COOH), and epoxy (-C-O-C) groups, which interact with water molecules through hydrogen bonding. The polar characteristics of carboxyl and hydroxyl functional groups improved water sorption on the membrane surface, facilitating water transport through the membrane matrix. This effect was further validated by different analyses, such as water uptake, swelling degree, and water contact angle measurements (Fig. 3), which demonstrated increased hydrophilicity with higher GO content.

Moreover, GO also contributed to the formation of a more porous and interconnected network within the membrane structure. The 2D nanosheet structure of GO acts as a physical spacer, preventing the compact packing of κC chains and creating additional free volume for water passage, leading to reduced resistance to water flux [35,42]. However, the gradual increase of GO concentration from kC-GO.01 (7.2 ± 0.15 L/m^{2}h) to kC-GO.03 (8.13 ± 0.17 L/M2H), followed by a smaller increment to kC-GO.04 (8.45 ± 0.17 L/m^{2}h) suggested that excessive GO loading could lead to partial agglomeration, which limited further improvement in water flux.

The membranes were assessed for water permeability and rejection of NaCl and $MgSO_4$ using 2 g/L NaCl and $MgSO_4$ solutions. The water flux for NaCl and $MgSO_4$ solutions followed a similar increasing trend with GO concentration but remained lower than that of DI water. The water flux showed an overall increase from 5.36 ± 0.20 L/m^{2}h to 7.42 ± 0.15 L/m^{2}h for NaCl and from 4.28 ± 0.10 L/m^{2}h to 6.37 ± 0.15 L/m^{2}h for $MgSO_4$. The hydrated ionic radii and charge density of the salt ions could be used to explain this difference (Fig. 6a). Na^+ ions (0.358 nm) are smaller and less hydrated than Mg^{2+} ions (0.428 nm), allowing NaCl to pass through the membrane with less resistance. Mg^{2+} was a possible form of crosslinker with κC, further decreasing water flux. Consequently, NaCl solutions generally experienced less resistance to water flow compared to $MgSO_4$ solutions, leading to a higher water flux through the hydrogel filter. Additionally, Mg^{2+} ions have a higher charge density, which leads to stronger electrostatic interactions with the negatively charged GO surface, limiting water passage and reducing the flux. The larger hydrated size of SO_4^{2-} (0.379 nm) compared to Cl^- (0.332 nm) further restricted the movement of $MgSO_4$ through the membrane pores, contributing to the lower water flux [14,43,44].

Fig. 6b shows the rejection performance of the κC and κC-GO membranes for both NaCl and $MgSO_4$ solutions. The rejection rates were notably high for both NaCl and $MgSO_4$, reflecting the membranes' strong ability to hinder the passage of these ions selectively. The high rejection performance could be attributed to several factors and separation mechanisms. Firstly, the intrinsic properties of κC itself contributed significantly to the membrane rejection capabilities. As a polysaccharide, κC forms a gel-like network with strong hydrogen bonding between its molecular chains, which helps to form a tight matrix that limits the passage of ions through size exclusion. Additionally, the natural negative charge of sulfated polysaccharide κC further enhances the rejection of positively charged ions like Na^+ and Mg^{2+} through electrostatic repulsion [14,45]. The crosslinking of κC with PEI further improves membrane stability and ion rejection by reinforcing the membrane structure and reducing its swelling tendency [46].

The incorporation of GO introduces functional groups that interact with ions through electrostatic forces, enhancing the membrane's selective permeability for ions like Na^+ and Mg^{2+}. GO also contributes to improved rejection performance through its size exclusion effect and by creating additional steric hindrance, limiting the passage of larger ions like Mg^{2+} and SO_4^{2-} [47].

For NaCl, the rejection increased from 84 ± 1 % (κC) to a peak of 93 ± 0.5 % for κC-GO.02, before slightly declining to 86 ± 1 % for κC-GO.03 and 82 ± 1.5 % for κC-GO.04. The increase in NaCl rejection with GO concentration is due to the stronger interaction between the negatively charged GO surface and Na^+ ions, which effectively hinders their passage through electrostatic repulsion, as well as the free volume affected by M_C, as discussed in the Supplementary Material. However, the subsequent decline of NaCl rejection at higher GO content suggests potential agglomeration of GO nanosheets, which may create defects or non-selective pathways that reduce the membrane's rejection efficiency. This agglomeration likely disrupts the electrostatic interactions and steric hindrance provided by GO [48].

For $MgSO_4$, the rejection improved from 89.45 ± 0.40 % for κC to a maximum of 97.13 ± 0.50 % for κC-GO.02, followed by a decrease to 93.6 ± 1 % for κC-GO.03 and 92.87 ± 0.80 % for κC-GO.04. The higher rejection rate for $MgSO_4$ compared to NaCl was consistent with the higher charge density and larger hydrated size of Mg^{2+} and SO_4^{2-} ions, which experienced stronger electrostatic interactions with the negatively charged GO surface. These interactions, along with the size exclusion mechanism, contributed to the higher rejection of $MgSO_4$. The observed decrease in $MgSO_4$ at higher GO content was again likely due to GO agglomeration, which disrupted the membrane's selectivity, reducing its ability to reject these ions efficiently [39]. In addition, while the high level of porosity along with high swelling at higher GO contents could facilitate the passage of water and increase the flux of solvent, they could also form pathways for the passage of solutes and thus reduce the efficiency of salt rejection. Among all the tested membranes, κC-GO.02 exhibited the highest rejection rates for monovalent and divalent salts, with a decent water flux of 7.72 ± 0.16 L/m^{2}h at 3 bar. The membrane performance from the water flux and salt rejection point of view, along with the balanced mechanical properties, could suggest that the κC-GO.02 membrane sample was the optimal membrane for wastewater treatment.

Experimental work demonstrated that increasing the concentration of GO led to the formation of interconnected nanochannels and interlayer gaps between the GO sheets, resulting in a larger porosity. Whilst GO sheets deposition in the pores will reduce their average size. Water flux in the kC-GO/PEI membrane increased with the GO concentration due to the greater membrane hydrophilicity (Fig. 3b) and GO agglomeration that creates gaps in the membrane structure. As a result, water flux increased, but at the expense of membrane selectivity caused by defects in the membrane structure, highlighting the trade-off between increased permeability and reduced rejection efficiency.

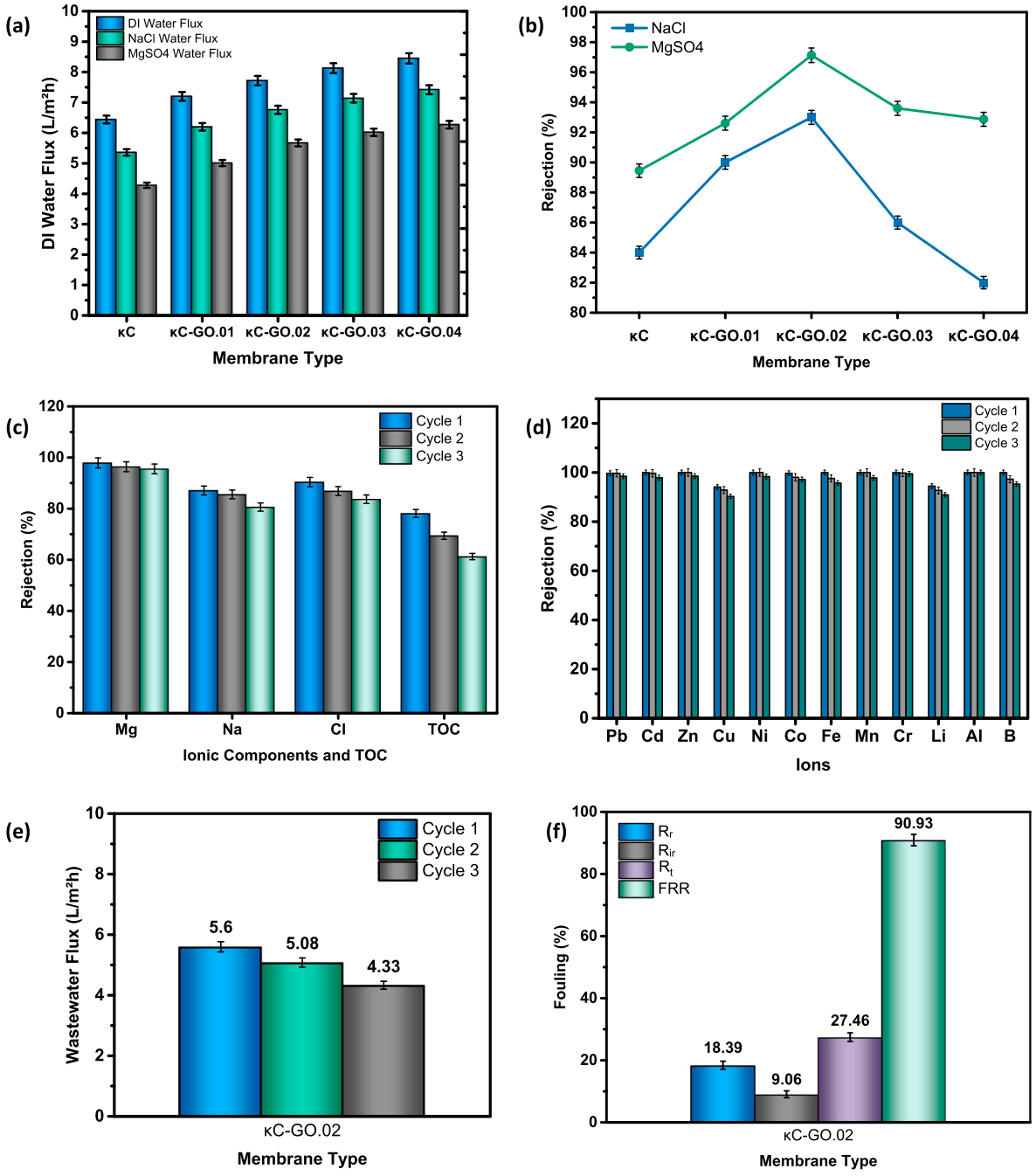


Fig. 6. (a) DI water, NaCl and $MgSO_4$ water flux, (b) NaCl and $MgSO_4$ (2 g/L) rejection, (c) Water flux for storm wastewater, (d) Ionic components and TOC rejection from the storm wastewater, (e) Rejection of heavy metal ions from the storm wastewater at 3 bar, (f) Fouling measurement.

3.5.2. Wastewater treatment

To further assess the performance of the optimal κC-GO.02 hydrogel membrane, stormwater was used as the feed solution over three filtration cycles. The initial feed composition and concentration are shown in Table 1. Due to the diverse particle sizes and complex nature of storm wastewater, the water flux was lower compared to pure water due to possibl1.7e pore blockage. The filtration process was conducted with a recovery rate of 50 %. Notably, the κC-GO.02 membrane achieved impressive ion rejection rates and a water flux of 5.6 L/m^2h in the first cycle at 3 bar.

As shown in Fig. 6c, the performance of the membrane for the removal of Total Organic Carbon (TOC), Na, Mg, and Cl from storm wastewater was evaluated over three filtration cycles. In the first cycle, the membrane achieved rejections of 97.89 ± 1.50 % for Mg, 87.1 ± 1.7 % for Na, 90.41 ± 2 % for Cl, and 78.1 ± 1.5 % for TOC. In the second cycle, the rejection slightly decreased to 96.41 ± 1.90 % for Mg, 85.55 ± 1.70 % for Na, 86.89 ± 1.70 % for Cl, and 69.4 ± 1.4 % for TOC. By the third cycle, the performance further declined to 95.55 ± 1.50 % for Mg, 80.62 ± 1.60 % for Na, 83.7 ± 1.7 % for Cl, and 61.26 ± 1.20 % for TOC. This gradual decline in rejection efficiency across multiple filtration cycles was indicative of membrane fouling and reduced active sites due to the accumulation of organic and inorganic matter on the membrane surface. However, the membrane still maintained relatively high rejection rates, especially for divalent ions like Mg^{2+}, due to the strong electrostatic interactions between the negatively charged GO surface and the high charge density of Mg^{2+} [14,44].

The κC-GO.02 membrane rejection of heavy metals is shown in Fig. 6d. In the first filtration cycle, the membrane achieved near-

complete removal of heavy metals, with 100 % rejection for cadmium (Cd), zinc (Zn), iron (Fe), manganese (Mn), chromium (Cr), aluminum (Al), boron (B), and nickel (Ni). Lead (Pb) and cobalt (Co) exhibited rejection rates of 99.7 ± 0.3 %, while copper (Cu) and lithium (Li) showed slightly lower rejection rates of 94.11 ± 0.90 % and 94.48 ± 0.70 %, respectively. Boron, which existed as boric acid at pH 5.3 (Table 1) in the feed, remained mostly uncharged in solution, making its rejection dependent on size exclusion and adsorption onto GO and weak mobility in the hydrogel. The lower rejection of Cu and Li could be attributed to the smaller hydrated radii of these ions (Li = 3.82 Å and Cu = 4.19 Å), which may allow them to pass through the membrane more easily compared to larger metal ions. These results were in agreement with the NaCl and $MgSO_4$ tests (Section 3.5.1), where divalent ions showed stronger rejection, while monovalent ions were more easily displaced, leading to lower rejection. Besides, Cu exhibited a higher binding affinity for oxygen-containing functional groups on GO and sulfate groups in κC. This strong interaction may reduce electrostatic repulsion, allowing Cu^{2+} to penetrate the filter matrix more effectively. Similarly, Li, being a monovalent ion with a high hydration energy, may interact less effectively with the charged functional groups, resulting in slightly lower rejection [49,50]. Li had a weak affinity for κC carboxyl (–COOH) and sulfate (–SO_3H) groups, allowing it to pass through the membrane more easily. On the contrary, heavy metals, such as Zn^{2+}, Cd^{2+}, and Cr^{3+}, form stronger complexes with –COOH and –SO_3H groups on the κC membrane. The rejection rate of most ions dropped in the following filtration cycles. Despite the slight decline in rejection rates over the subsequent filtration cycles, the membrane maintained a considerably efficient performance, which could be attributed to the synergistic effects of the κC matrix and GO additives.

The membrane effectively removed heavy metal ions through a combination of adsorption on the GO surface area, electrostatic repulsion of metal cations by the negatively charged sulfate groups in κC, especially at lower pH (Table 1). Also, heavy metal removal was likely achieved by complexation with sulfate groups (-OSO_3^-) in κC and oxygen-containing functional groups in GO, ion exchange that involved replacement of Na^+ and K^+ on carrageenan with heavy metals, and pore size exclusion. For κC, abundant sulfate (-OSO_3^-) and hydroxyl (-OH) groups facilitated strong electrostatic interactions and chelation with heavy metal ions. An example of this is the adsorption and chelation of Pb^{2+} ions, where the sulfate groups in κC electrostatically attract Pb^{2+} ions, forming a stable complex [51]:

$$Pb^{2+} + 2(-OSO_3^-) \rightarrow (-OSO_3)_2Pb \quad (11)$$

In addition to κC, GO played a critical role in heavy metal removal through surface interaction and adsorption. GO provided a high surface area and oxygen-containing functional groups, such as carboxyl (-COOH) and hydroxyl (-OH), which adsorbed heavy metals through surface complexation and electrostatic interactions. For example, Cr(VI) (chromate ions, CrO_4^{2-}) could be adsorbed by the carboxyl groups on GO, forming a surface complex:

$$Cr^{3+} + 3(-COO^-) \rightarrow (-COO)_3Cr \quad (12)$$

Furthermore, PEI contributed to heavy metal removal through complexation and ion exchange. PEI contains amine groups (-NH_2) that form strong coordination bonds with heavy metal ions and acted as ion exchange sites. For instance, Cu^{2+} (copper ions) could form coordination complexes with the amine groups of PEI [52]:

$$Cu^{2+} + -NH_2 \rightarrow -NH_2 - Cu^{2+} \quad (13)$$

Finally, the pore size exclusion mechanism further contributed to the rejection of heavy metals. The incorporation of GO and PEI into the κC matrix reduced the membrane's pore size and increased contaminants' rejection. According to Eq. (10), the pore size decreased from 2.45 nm for the pristine κC to 1.82 nm for the κC-GO.02 membrane. This reduction in pore size limited the passage of larger hydrated metal ions. For example, hydrated Pb^{2+} ($Pb(H_2O)_6^{2+}$), with an effective size larger than the membrane pores, was physically blocked from passing through [53].

It is worth mentioning that while adsorption contributes to ion removal, it was not the dominant mechanism in this membrane. Instead, size exclusion, electrostatic repulsion, chemical affinity, and Donnan effects account for the high rejection observed. This distinction explained why designed nanocomposite membranes outperformed bulk hydrogel adsorbents, which rely mainly on chemical binding and require regeneration that produces secondary waste streams. In terms of selectivity, the size and distribution of pores and surface charge define the nanocomposite membrane rejection performance, while pore size and functional groups determine the selectivity of adsorbents [54]. Lastly, regeneration of the adsorbents results in a secondary stream of wastewater, which increases the cost of treatment. Therefore, the nanocomposite membrane was a better option for wastewater treatment.

Practically, the κC -GO.02 membrane contained a small amount of 0.02 %*w/v* of GO that reduced its cost, while optimizing its performance. Increasing the concentration of GO to 0.04 %w/v not only compromised the membrane performance due to GO agglomeration, but also increased the membrane cost. The GO coating on the surface of the κC membrane was designed to enhance its antifouling properties and for the rejection of divalent ions by mechanisms such as electrostatic repulsion, size exclusion, and binding through the oxygen groups. Li, B, and Na, on the other hand, have low affinity to GO due to the limited cation-π interaction and strong hydration shell. Accordingly, the rejection of these ions was possibly attributed to the κC crosslinked with the PEI membrane. The negatively charged κC -PEI layer, with a small pore size, restricted the transportation of Li, B (as boric acid at pH 5.3), and Na via size exclusion, hydrogen bonding, and electrostatic interaction.

3.5.3. *Antifouling studies*

Membrane fouling is a major challenge in water treatment, causing a decline in permeate flux due to the accumulation of foulants such as organic matter, heavy metals, and particulates on the membrane surface [55]. Stormwater containing heavy metals was used as the feed solution over three filtration cycles to evaluate the antifouling properties of the κC-GO.02 hydrogel membrane, and DI water is used for membrane washing between cycles. The membrane structure remained intact during the repeated cycles, and rinsing with DI water followed by drying between runs helped preserve the active layer without visible delamination or surface degradation. The experiments were conducted at 3 bars and room temperature in a dead-end filtration mode.

The membrane initially exhibited a water flux of 5.6 ± 0.2 L/m^2h in the filtration cycle, which declined to 5.08 ± 0.15 L/m^2h in the second filtration cycle, and further decreased to 4.33 ± 0.14 L/m^2h in the third cycle (Fig. 6e). This decline could be attributed to the accumulation of fouling materials on the membrane surface, as shown in the EDX results (Table 3), leading to partial pore blockage and increased resistance to water flow. However, after each cycle, DI water washing was performed to remove weakly adhered foulants, demonstrating the membrane's ability to recover membrane performance. The flux recovery ratio (FRR) was 90.93 %, indicating the strong antifouling capability of the κC-GO.02 membrane and the effectiveness of the cleaning process.

Fig. 6f presents the total resistance (R_t), reversible resistance (R_r), and irreversible resistance (R_{ir}) of the κC-GO.02 membrane. The total resistance (R_t) was 27.46 %, with 18.39 % attributed to reversible fouling (R_r) and 9.06 % to irreversible fouling (R_{ir}). The relatively high reversible fouling fraction suggested that a significant portion of contaminants adhered loosely to the membrane and were successfully removed through DI water washing.

The antifouling performance of the membrane was largely attributed to the combined effects of κC and GO. κC, as a hydrophilic biopolymer, enhanced water permeability and reduced the adhesion of hydrophobic foulants, limiting irreversible fouling. Additionally, the presence of GO contributed to the membrane's negative surface charge, which repelled

certain contaminants, particularly heavy metals and organic matter, further preventing their accumulation. In addition, the small pore size of the membrane prevented the pollutants from entering the pores within the membrane structure, which facilitated the efficiency of washing. The synergistic effect of these components allowed the κC-GO.02 membrane to maintain stable performance over multiple cycles despite cleaning with DI water only, making it a promising candidate for stormwater treatment and heavy metal removal applications.

It is noteworthy that there is no standard method for fouling tests for a new membrane, such as the number of filtration cycles, the length of cycles, membrane cleaning, and recovery rate. Typically, long-term performance and cleaning protocol of a new membrane would be developed over time based on the parameters mentioned above, as well as the type of feed solution. In this study, the fouling tests were conducted in filtration cycles at a 50 % recovery rate and cleaning with DI water only. The tests demonstrated that the developed membrane enjoys excellent antifouling properties, retaining more than 90 % of its original flux after three filtration cycles and cleaning with DI water only. Irreversible fouling in three filtration cycles was 9 % only, indicating excellent water flux recovery.

3.5.4. Performance comparison

This study is the first attempt that succeeded in fabricating a composite κC-GO membrane of competitive rejection and water flux compared to the literature (Table 4). The κC-GO.02 membrane exhibited excellent performance, represented by its exceptional antifouling properties and rejection of heavy metals. This high rejection was attributed to the synergistic effects of GO and PEI, which enhanced crosslinking, increased active sites, and reinforced the hydrogel structure. Although previous hydrogel membranes demonstrated high water flux, they struggled with achieving high rejection rates for both divalent and monovalent ions. For instance, a CaAlg-based hydrogel membrane achieved a flux of 43.2 L/m^{2}h, but its rejection rates were below 8 % for monovalent ions, such as NaCl [51]. In a study by Karbassiyazdi et al. [9], a CA carbon-based aluminum hydrogel membrane showed excellent rejection of divalent ions but compromised rejection of NaCl and mechanical strength. In another work, a GO-based membrane with MoS_2 spacers was fabricated to reject ≥95 % of dyes that showed moderate ion rejection, including 43.2 % of NaCl, 65.2 % of Na_2SO_4, 26.5 % of $MgCl_2$, and 24.3 % of $MgSO_4$. In comparison, the κC-GO.02 membrane in this research exhibited excellent rejection of both monovalent ions (>93 %) and divalent ions (>97 %) at a feed pressure of 3 bar. The membrane successfully treated stormwater, removing almost all traces of Cd, Zn, Fe, Mn, Cr, Al, B, and Ni. It also achieved 99.7 % rejection for Pb and Co, while Cu and Li showed slightly lower removal rates of 94.11 % and 94.48 %, respectively. The membrane maintained a consistent rejection rate across multiple filtration cycles, showcasing stable performance and preferential antifouling characteristics.

The tight molecular structure nanofiltration κC-GO.02 membrane exhibited better rejection to NaCl, 93 %, than the commercial tight molecular structure NF membranes, making it suitable for the treatment of wastewater containing divalent and monovalent ions. For example, the Toray NE8040–70 NF membrane, with 30 % to 70 % NaCl rejection and 98 % to $MgSO_4$, and the Trisep TS80 NF membrane, with 80 % rejection to NaCl and 98.5 % to $MgSO_4$, are applicable for wastewater treatment, but their rejection to monovalent ions is compromised. In contrast, the κC-GO.02 demonstrated excellent rejection to divalent and monovalent ions, including Li and B, that are challenging to remove and recover by the commercial NF membrane. Importantly, the κC-GO.02 was constituted of natural and biodegradable materials, suggesting a lower environmental footprint at end-of-life compared with commercial polyamide or polysulfone NF membranes, which are non-biodegradable and contribute to persistent plastic waste. Moreover, future work should explore recycling or reuse strategies to improve the sustainability of hydrogel-based membranes further.

4. Conclusion

In this study, κC-based hydrogels were modified by incorporating varying concentrations of GO (0.01 to 0.04 %) to improve water flux and rejection performance. The study investigated the effects of GO concentration on the membrane's structural properties, water flux, and ion rejection capabilities. GO incorporation enhanced the membrane's water permeability, which was attributed to the polar functional groups of GO and its ability to create a more porous membrane structure. The study also demonstrated the positive impact of GO on the hydrophilicity of the membranes, further supporting the improved water transport efficiency.

The water flux and rejection performance were evaluated using various salt solutions, including NaCl and $MgSO_4$, and the κC-GO membranes showed promising results. As GO concentration increased from 0.01 % to 0.04 %, water flux improved. The κC-GO.02 membrane achieved a water flux of 7.72 L/m^{2}h, which was a 20 % increase compared to the pure κC membrane's flux of 6.44 L/m^{2}h. However, higher GO concentrations, enhancement in water flux occurred due to higher swelling and hydrophilicity, but particularly for 0.03 % and 0.04 % content, slight agglomeration occurred, which limited further enhancement of ion rejection due to possible formation of pathways that could facilitate the passage of salts. The same trend was also observed for mechanical properties, where a high GO content reduced tensile strength and the κC-GO.02 sample showed the best mechanical strength. The rejection rates for both NaCl and $MgSO_4$ were high, with the κC-GO.02 membrane achieving a NaCl rejection of 93 % and an $MgSO_4$ rejection of 97.13 %, both among the highest observed in the study. The membrane also showed excellent performance in storm wastewater treatment, maintaining high rejection rates for heavy metals and organic contaminants. For example, the κC-GO.02 membrane achieved over 99 % removal of Cd, Zn, Fe, Mn, Cr, Al, B, and Ni, with Pb and Co at 99.7 %, while Cu and Li showed slightly lower rejection rates of 94.11 % and 94.48 %, respectively. Despite some reduction in performance due to fouling, the membrane demonstrated promising stability.

In conclusion, the designed κC-GO nanocomposite hydrogel membrane demonstrated excellent performance in terms of water flux, ion rejection, and heavy metal removal, making it a potential candidate for wastewater treatment applications. Future work could focus on exploring long-term stability under real-world conditions and testing the membrane's performance with more complex wastewater matrices to improve its efficiency and practical application further. Also, nanoscale water flux through a GO-crystalline hydrogel membrane can be studied using molecular dynamic simulation or related atomistic models.

CRediT authorship contribution statement

Rokhsare Kardani: Writing – review & editing, Writing – original draft, Validation, Investigation, Formal analysis, Data curation, Conceptualization. **Ali Altaee:** Writing – review & editing, Validation, Supervision, Resources, Formal analysis, Data curation. **Armaghan Moghaddam:** Writing – review & editing, Validation, Formal analysis, Data curation. **Hossein Ali Khonakdar:** Writing – review & editing, Validation, Formal analysis, Data curation. **Akshaya K. Samal:** Validation, Formal analysis, Data curation, Conceptualization. **John Zhou:** Validation, Supervision, Formal analysis, Data curation. **Youngwoo Choo:** Investigation, Formal analysis.

Declaration of competing interest

The authors declare that they have no known competing financial interests or personal relationships that could have appeared to influence the work reported in this paper.

Table 4
Performance of various membranes made for wastewater treatment and their water flux and rejection rate.

Type of hydrogel membrane	Feed	Feed Concentration (mg/L)	Pure Water Flux (L/m^2h)	Pressure (bar)	Rejection (%)	Reference
PA-TFC-I (PVA interlayered)	NaCl	2000	28.2	1	46.2	[56]
PA-TFC-P (PVA coated)	Na_2SO_4		9.4		38.5	
PA-TFC-C (Pristine)			8.8		33.3	
					99.8	
					99.4	
					98.8	
GO-MoS_2/PVDF	NaCl	1 (mM)	10.2	1	43.2	[57]
	Na_2SO_4				65.2	
	$MgCl_2$				26.5	
	$MgSO_4$				24.3	
PEI-TMC-Polyamide	NaCl	1000	17.2	8	27.8	[58]
	Na_2SO_4				90.4	
	$MgCl_2$				92.4	
	$MgSO_4$				93.6	
CA, carbon-based aluminum hydroxide (CACG)	Pb	1000	30	0.015 (Gravity)	97.4	[10]
	Cu				95	
	Ca				29.5	
	Mg				84.5	
	Mn	0.1			93	
	Ni	3.27			99.6	
	Zn	4.4			96	
	Pb	6.63			98.3	
	As	5.69			99.9	
	Cu	6.27			96	
PES-Chitosan and 1,3,5-triglycidyl isocyanurate (TGIC)	Mg	500	47.88	6	94.2	[59]
CaAlg-polyacrylamide	BSA	500	25	1	98.53	[60]
		100			99.64	
r-HGO	Na_2SO_4	2000	6.6	1	98.5	[61]
Ba^{2+}/ Ca^{2+}/– NaAlg	Methyl blue	60	43.5	1	99.6	[62]
	Na	1000			8.2	
Ca^{2+}/– NaAlg - PAAm- PEG-POSS	Methyl blue	500	11.7	2	93	[63]
	Congo red				95	
NaAlg - PEG- CNF- MWCNT-COOH	Crystal Violet	100	51.6	1	99.8	[64]
	Congo red				98.9	
	Tartrazine				93.1	
	Methyl blue				85.7	
	$MgSO_4$	500			11.6	
	Na_2SO_4				10.5	
	$MgCl_2$				9.1	
	NaCl				7.3	
κC-nano Zero Valent Iron- PEI	NaCl	2000	18	2.06	90.96	[65]
	$MgSO_4$				98.83	
	Cd	1.64			99.82	
	Pb	1.71			98.68	
	Al	1.78			99.46	
	Cr	1.78			99.53	
	Mn	1.83			99.96	
	Li	2.07			98.85	
	Co	1.72			100	
	Ni	1.68			99.72	
	Cu	1.76			99.91	
	Zn	1.84			100	
GO-NFM	NaCl	0.02 M	11.13	1	27.86	[66]
	Na_2SO_4				63.13	
	$MgCl_2$				15	
	$MgSO_4$				41.82	
κC-GO- PEI	NaCl	2000	7.72	3	93	This Work
	$MgSO_4$				97.13	
	Cd	0.8			100	
	Pb	0.78			99.7	
	Al	0.45			100	
	Cr	0.525			100	
	Mn	0.8			100	
	Li	0.84			94.48	
	Co	0.77			99.7	
	Ni	0.76			100	
	Cu	0.82			94.11	
	Zn	0.8			100	
	Fe	0.23			100	
	B	0.48			100	

Appendix A. Supplementary data

Supplementary data to this article can be found online at https://doi.org/10.1016/j.cej.2025.168932.

Data availability

Data will be made available on request.

References

[1] D. Trishitman, et al., Reverse osmosis for industrial wastewater treatment, in: Current Trends and Future Developments on (Bio-) Membranes, 2020, pp. 207–228.
[2] B.-M. Jun, et al., Applications of metal-organic framework based membranes in water purification: a review, Sep. Purif. Technol. 247 (2020).
[3] N. Mancosu, et al., Water scarcity and future challenges for food production, Water 7 (12) (2015) 975–992.
[4] Z. Yang, et al., A review on reverse osmosis and nanofiltration membranes for water purification, Polymers (Basel) 11 (8) (2019).
[5] R. Kardani, et al., Mesoporous copper zinc bimetallic imidazolate MOF as nanofiller to improve gas separation performance of PEBA-based membranes, J. Ind. Eng. Chem. 83 (2020) 100–110.
[6] R. Kardani, et al., Effects of nanofillers on the characteristics and performance of PEBA-based mixed matrix membranes, Rev. Chem. Eng. 34 (6) (2018) 797–836.
[7] P. Mohammadzadeh Pakdel, S.J. Peighambardoust, A review on acrylic based hydrogels and their applications in wastewater treatment, J. Environ. Manage. 217 (2018) 123–143.
[8] M.K. Yazdi, et al., Hydrogel membranes: a review, Mater. Sci. Eng. C Mater. Biol. Appl. 114 (2020) 111023.
[9] Y. Chen, et al., Green multifunctional PVA composite hydrogel-membrane for the efficient purification of emulsified oil wastewater containing Pb(2+) ions, Sci. Total Environ. 856 (Pt 2) (2023) 159271.
[10] E. Karbassiyazdi, et al., Gravity-driven composite cellulose acetate/activated carbon aluminium-based hydrogel membrane for landfill wastewater treatment, Chem. Eng. Res. Des. 200 (2023) 682–692.
[11] F. Ahmad, et al., An eco-friendly hydroentangled cotton non-woven membrane with alginate hydrogel for water filtration, Int. J. Biol. Macromol. 256 (Pt 1) (2024) 128422.
[12] S. Radoor, et al., Carrageenan/calcium alginate composite hydrogel filtration membranes for efficient cationic dye separation, Int. J. Biol. Macromol. 270 (Pt 2) (2024) 132309.
[13] K. Zhao, et al., Anti-fouling and anti-bacterial graphene oxide/calcium alginate hybrid hydrogel membrane for efficient dye/salt separation, Desalination 538 (2022).
[14] S. Yadav, et al., Surface modification of nanofiltration membrane with kappa-carrageenan/graphene oxide for leachate wastewater treatment, J. Membr. Sci. 659 (2022).
[15] I. Ibrar, et al., Kappa carrageenan-vanillin composite hydrogel for landfill leachate wastewater treatment, Desalination 565 (2023).
[16] C. Alvarez-Lorenzo, et al., Crosslinked ionic polysaccharides for stimuli-sensitive drug delivery, Adv. Drug Deliv. Rev. 65 (9) (2013) 1148–1171.
[17] S. Deng, Y.P. Ting, Characterization of PEI-modified biomass and biosorption of Cu (II), Pb(II) and Ni(II), Water Res. 39 (10) (2005) 2167–2177.
[18] P. Fei, et al., Quantitative analysis of cellulose acetate with a high degree of substitution by FTIR and its application, Anal. Methods 9 (43) (2017) 6194–6201.
[19] W. Wang, et al., Designing bioinspired nanofiltration membrane for enhanced water permeance and efficient ion sieving, Chem. Eng. J. 483 (2024) 149376.
[20] L. Shao, et al., PVA/polyethyleneimine-functionalized graphene composites with optimized properties, Mater. Des. 99 (2016) 235–242.
[21] H. Mokhtari, et al., An injectable mechanically robust hydrogel of Kappa-carrageenan-dopamine functionalized graphene oxide for promoting cell growth, Carbohydr. Polym. 214 (2019) 234–249.
[22] S. Yadav, et al., Preparation of novel high permeability and antifouling polysulfone-vanillin membrane, Desalination 496 (2020).
[23] S.M. Husna, et al., Effect of graphene oxide on the properties of polymer inclusion membranes for gold extraction from acidic solution, Membranes (Basel) 12 (10) (2022).
[24] S. Zheng, et al., Swelling of graphene oxide membranes in aqueous solution: characterization of interlayer spacing and insight into water transport mechanisms, ACS Nano 11 (6) (2017) 6440–6450.
[25] S. Liu, H. Bao, L. Li, Thermoreversible gelation and scaling laws for graphene oxide-filled κ-carrageenan hydrogels, Eur. Polym. J. 79 (2016) 150–162.
[26] K. Deshmukh, S.M. Khatake, G.M. Joshi, Surface properties of graphene oxide reinforced polyvinyl chloride nanocomposites, J. Polym. Res. 20 (11) (2013).
[27] M. Yang, et al., Preparation of graphene oxide modified poly(m-phenylene isophthalamide) nanofiltration membrane with improved water flux and antifouling property, Appl. Surf. Sci. 394 (2017) 149–159.
[28] R. Mukherjee, P. Bhunia, S. De, Impact of graphene oxide on removal of heavy metals using mixed matrix membrane, Chem. Eng. J. 292 (2016) 284–297.
[29] Y.-C. Chiang, et al., Nanofiltration membranes synthesized from hyperbranched polyethyleneimine, J. Membr. Sci. 326 (1) (2009) 19–26.
[30] A. Moghaddam, S. Mehdipour-Ataei, S. Babanzadeh, Novel poly (ether sulfone isopropyl sulfide) support layer in thin film composite membrane for desalination, Chemical Eng. J. Adv. (2025) 100717.
[31] D. Moncada, et al., Injectable carrageenan/green graphene oxide hydrogel: a comprehensive analysis of mechanical, rheological, and biocompatibility properties, Polymers (Basel) 16 (16) (2024).
[32] M. Nasr, et al., Preparation, characterization, and performance of PES/GO woven mixed matrix nanocomposite forward osmosis membrane for water desalination, RSC Adv. 12 (39) (2022) 25654–25668.
[33] H. Jahandideh, et al., Fabrication of graphene-based porous materials: traditional and emerging approaches, Chem. Sci. 13 (31) (2022) 8924–8941.
[34] A. Khosrozadeh, et al., Wettability and sound absorption of graphene oxide doped polymer hydrogel, Sci. Rep. 11 (1) (2021) 15949.
[35] A. Marjani, et al., Effect of graphene oxide on modifying polyethersulfone membrane performance and its application in wastewater treatment, Sci. Rep. 10 (1) (2020) 2049.
[36] S.C. Lee, et al., Physical and chemical factors influencing the printability of hydrogel-based extrusion bioinks, Chem. Rev. 120 (19) (2020) 10834–10886.
[37] T. He, et al., Three-dimensional graded porous structure and compressible KGM-GO/CS/SA composite aerogel spheres for efficient adsorption of antibiotics, Sep. Purif. Technol. 346 (2024) 127547.
[38] C.M.B. de Araujo, et al., Wastewater treatment using recyclable agar-graphene oxide biocomposite hydrogel in batch and fixed-bed adsorption column: bench experiments and modeling for the selective removal of organics, Colloids Surf. A Physicochem. Eng. Asp. 639 (2022) 128357.
[39] S.K. Tiwary, et al., Graphene oxide-based membranes for water desalination and purification, NPJ 2D Mater. Appl. 8 (1) (2024).
[40] M.D. Ong, et al., Modification of cellulose acetate microfiltration membranes using graphene oxide-polyethyleneimine for enhanced dye rejection, Membranes (Basel) 13 (2) (2023).
[41] X. Chen, et al., Preparation and perfomance of an aging-resistant nanocomposite film of binary natural polymer-graphene oxide, ACS Omega 1 (6) (2016) 1173–1181.
[42] C. Dai, et al., Impact of graphene oxide on properties and structure of thin-film composite forward osmosis membranes, Polymers (Basel) 14 (18) (2022).
[43] B. Tansel, et al., Significance of hydrated radius and hydration shells on ionic permeability during nanofiltration in dead end and cross flow modes, Sep. Purif. Technol. 51 (1) (2006) 40–47.
[44] W. Cheng, et al., Selective removal of divalent cations by polyelectrolyte multilayer nanofiltration membrane: role of polyelectrolyte charge, ion size, and ionic strength, J. Membr. Sci. 559 (2018) 98–106.
[45] L. Alsaka, et al., A review of hydrogel application in wastewater purification, Separations 12 (2) (2025).
[46] M.M. Elnashar, T. Kahil, Biopolymeric formulations for biocatalysis and biomedical applications, Biomed. Res. Int. 2014 (2014) 418097.
[47] S. Yadav, et al., Preparation of fouling resistant and highly perm-selective novel PSf/GO-vanillin nanofiltration membrane for efficient water purification, J. Hazard. Mater. 421 (2022) 126744.
[48] S. Sali, H.R. Mackey, A.A. Abdala, Effect of graphene oxide synthesis method on properties and performance of polysulfone-graphene oxide mixed matrix membranes, Nanomaterials (Basel) 9 (5) (2019).
[49] A. Razmjou, et al., Design principles of ion selective nanostructured membranes for the extraction of lithium ions, Nat. Commun. 10 (1) (2019) 5793.
[50] P.R. Irving, et al., Engineering lithium-magnesium selectivity in hydrated polymer membranes through polymer backbone rigidity, ACS Macro Lett. 14 (2) (2025) 161–168.
[51] K. Kalaiselvi, et al., Adsorption of Pb2+ ions from aqueous solution onto porous kappa-carrageenan/cellulose hydrogels: isotherm and kinetics study, Sustainability 15 (12) (2023).
[52] J. Geng, et al., Polyethyleneimine cross-linked graphene oxide for removing hazardous hexavalent chromium: adsorption performance and mechanism, Chem. Eng. J. 361 (2019) 1497–1510.
[53] A.E.D. Mahmoud, E. Mostafa, Nanofiltration membranes for the removal of heavy metals from aqueous solutions: preparations and applications, Membranes (Basel) 13 (9) (2023).
[54] J. Qiao, et al., Sodium alginate-based nanocomposite hydrogel membrane for removal of heavy metal ions and dyes in water, Int. J. Biol. Macromol. 307 (2025) 142109.
[55] C.P. Sharma, Z. Zhu, A. Ronen, Membrane Filtration for Wastewater Treatment–Fouling Mitigation, 2024.
[56] X. Zhu, et al., Toward tailoring nanofiltration performance of thin-film composite membranes: novel insights into the role of poly(vinyl alcohol) coating positions, J. Membr. Sci. 614 (2020).
[57] P. Zhang, et al., Novel "loose" GO/MoS2 composites membranes with enhanced permeability for effective salts and dyes rejection at low pressure, J. Membr. Sci. 574 (2019) 112–123.
[58] Z. Yang, et al., Novel polyethyleneimine/TMC-based nanofiltration membrane prepared on a polydopamine coated substrate, Front. Chem. Sci. Eng. 12 (2) (2017) 273–282.
[59] B. Yang, et al., Chitosan nanofiltration membranes with gradient cross-linking and improved mechanical performance for the removal of divalent salts and heavy metal ions, Desalination 516 (2021).
[60] X. Zhang, et al., A free-standing calcium alginate/polyacrylamide hydrogel nanofiltration membrane with high anti-fouling performance: preparation and characterization, Desalination 365 (2015) 234–241.

[61] X. Chen, et al., Reduced holey graphene oxide membranes for desalination with improved water permeance, ACS Appl. Mater. Interfaces 12 (1) (2020) 1387–1394.
[62] N. Gao, et al., Ba2+/Ca2+ co-crosslinked alginate hydrogel filtration membrane with high strength, high flux and stability for dye/salt separation, Chin. Chem. Lett. 35 (5) (2024).
[63] J. Hu, et al., A self-supported gel filter membrane for dye removal with high anti-fouling and water flux performance, Polymer 201 (2020).
[64] R. Cai, et al., Self-supported hydrogel loose nanofiltration membrane for dye/salt separation, Sep. Purif. Technol. 328 (2024).
[65] R. Kardani, et al., Eco-friendly kappa-carrageenan-nano zerovalent iron hydrogel water and wastewater purification, J. Hazard. Mater. 492 (2025) 138123.
[66] L. Chen, et al., High performance graphene oxide nanofiltration membrane prepared by electrospraying for wastewater purification, Carbon 130 (2018) 487–494.
[67] L. Alsaka, Kappa-carrageenan-based hydrogel for leachate wastewater treatment and resource recovery, Desalination 614 (2025) 119208.